PCCP

Accepted Manuscript

ROYAL SOCIETY OF CHEMISTRY

www.rsc.org/pccp

Physical Chemistry Chemical Physics RSCPublishing

ARTICLE

A DFT Study on Reaction Mechanism of Dimerization of Methyl Methacrylate Catalyzed by N-Heterocyclic Carbene

Cite this: DOI: 10.1039/x0xx00000x

Received 19th May 2014,
Accepted 28th July 2014

DOI: 10.1039/x0xx00000x

www.rsc.org/

Yunxia Li,[a] Yanyan Zhu[a,*], Wenjing Zhang[a], Donghui Wei[a,*], Yingying Ran[a], Qilin Zhao[a] and Mingsheng Tang[a]

Abstract: Reaction mechanisms of the N-heterocyclic carbene (NHC)-catalyzed dimerization of methyl methacrylate were studied using density functional theory (DFT) at the M05-2X/6-31G(d,p) level of theory. Four possible reaction channels (A, B, C, and D) have been investigated in this work. Particularly, we proposed a novel reaction pathway, where the proton transfers are assisted by a different molecule. The calculated results indicate that the channels B and D are more energetically favourable channels. The obtained results suggest that E-isomer product is the main product, which is in agreement with the experimental results. Further calculations and analyses of global and local reactivity indices reveal the role of the NHC catalysts in the title reaction. The obtained mechanistic insights are valuable for not only rational design of more efficient NHC catalysts but also understanding the similar reaction mechanism.

Introduction

The chemistry of N-heterocyclic carbenes (NHCs) has grown rapidly in the past decades.[1] NHCs are now important ligands in homogeneous catalysis that show better catalytic activities than typical phosphines in a number of transition metal catalyzed organic transformations.[2] Due to the extensive utilization of NHCs in organocatalysts, NHCs have been used in more and more reactions as effective catalysts to replace the enzymatic and organometallic catalysis.[3] Recently, NHCs have become the most promising catalysts to catalyze dimerization.[4]

Take the tail-to-tail dimerization of substituted olefins into account, the expected dimers are potential precursors to monomers for condensation polymerization in synthesizing intermediates for fine and commodity chemicals.[5] Pertaining to its wide range of applications, many transition metal complexes have been reported to catalyze the dimerization of methyl acrylate andacrylonitrile.[6] For instance, Kashiwagi and co-workers invented an effective Ru catalysts for the dimerization of acrylonitrile in the presence of carboxylic acids.[7] Subsequently, Hirano's group reported an active Ru catalysts for the tail-to-tail dimerization of methyl methacrylate[8] and methyl acrylate,[9] respectively. However, these organometallic catalytic dimerization reactions do not always lead to good yields of the expected products. Therefore, much effort has been focused on NHCs as an organocatalysts to improve the reaction selectivity and to expand the substrate scope of dimerization.[10] Glorius and Matsuoka groups reported the dimerization of aldehydes and alkenes in experiment.[11] Chen et al. carried out the computational mechanistic studies on organocatalytic Conjugate-Addition polymerization of linear and cyclic acrylic monomers by N-heterocyclic carbenes.[12]

Noteworthy, Matsuoka and co-workers found that in the presence of catalytic amounts of NHC (the specific NHC chosen for the experiment, denoted Cat in Scheme 1), methyl methacrylate (simplified as MMA in the following text) was selectively converted to the tail-to-tail dimer with an E/Z ratio of 95:5 with a yield of 85% at 80°C in toluene.[13]

According to the mechanism proposed by Matsuoka and co-workers, six steps are involved (shown in Scheme 2). Although the intermediates M2 and M4 (depicted in Scheme 2) have been detected via the ESI-MS spectroscopy in the experiment,[13] the reaction mechanism of NHC-catalyzed dimerization is still obscure. Some of the steps in the proposed mechanism are questionable. The direct intramolecular 1,2-H shift (depicted in Scheme 2) is very difficult to take place under the experimental conditions due to the strain of the three-membered ring in transition state.[14] How does the NHC-catalyzed dimerization take place under the experimental conditions? How do the proton transfers proceed? Why is the E-isomer the main

product? Challenges to answer all these questions motivate the present work.

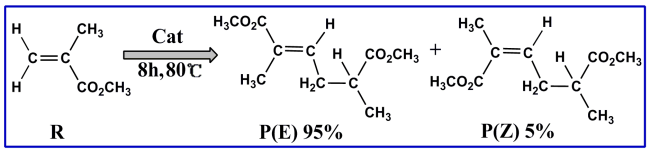

Scheme 1 The NHC-catalyzed dimerization.

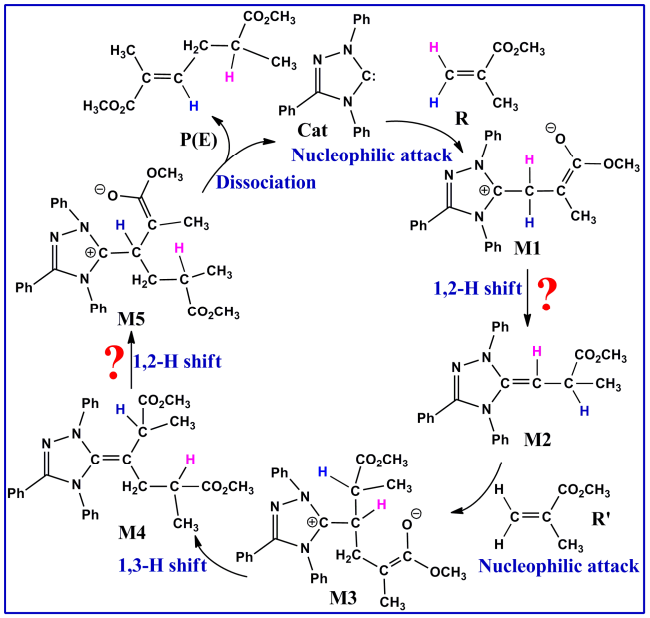

Scheme 2 The possible mechanism reported in experiment.[13]

In this work, all computational models were selected on the basis of the experimental results. As it states, MMA (denoted R in Scheme 1), the N-heterocyclic carbene (denoted Cat in Scheme 1) and the products (denoted P(E) and P(Z) in Scheme 1) were chosen as the objects of the investigation. The detailed mechanisms were investigated using the density functional theory (DFT), which has been widely used in the study of reaction mechanism.[15]

Computational details

All theoretical calculations were performed using the Gaussian 09 program.[16] Specifically, the structural and energetic results calculated by M05-2X are more consistent with the experimental observations than those by other DFT functions.[17] The M05-2X function was thus selected to carry the DFT calculation.[18] All structures were optimized and characterized as energy minima at the M05-2X/6-31G(d, p) level of theory. Vibrational frequency calculations were then performed based on the optimized geometries at the same level, so as to confirm that all the reactants, intermediates and products have no imaginary frequencies, and each transition state has one and only one imaginary frequency. The intrinsic reaction coordinate (IRC) calculations,[19] at the same level of theory, were performed to ensure that the transition states lead to the expected reactants and products. The energetic results were then refined by the single-point calculations at M05-2X/6-311++G(2d, 2p) level with the solvent effect of toluene using the integral equation formalism polarizable continuum solvent model (IEFPCM).[20] Natural bond orbital (NBO)analyses were performed with the same basis set to assign the atomic charges.[21] All energies reported in this paper include the zero-point vibrational energy (ZPVE) corrections obtained from the frequency calculations at the M05-2X/6-31G(d, p) level of theory.

Results and discussion

Four possible reaction channels.

For the title reaction, we have suggested and studied four possible reaction channels (A, B, C, and D, as depicted in Scheme 3) on the basis of experimental results. The calculated potential energy profiles for the four reaction channels are presented in Figure 1. The energy of Cat+R+R′ is set as 0.00 kcal/mol as reference for the potential energy profiles. Furthermore, Figure 2 to Figure 5 present all the optimized structures involved in channels A, B, C, and D.

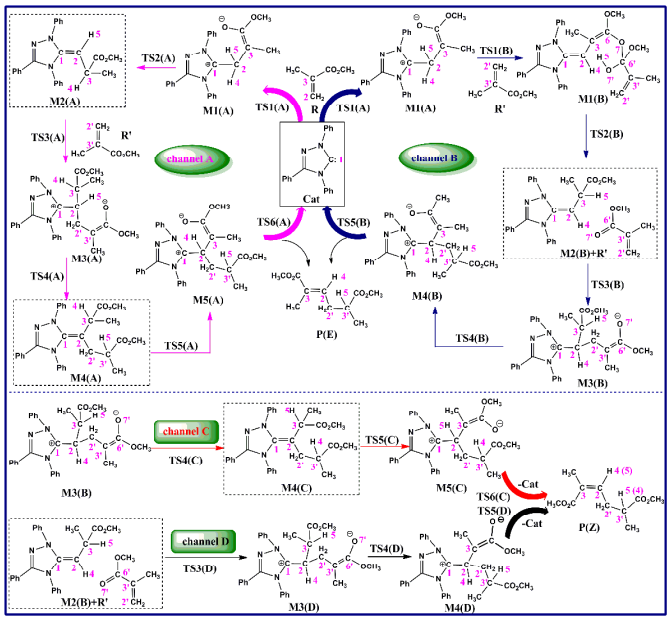

Scheme 3 The possible reaction channels (A, B, C, and D) of the title reaction.

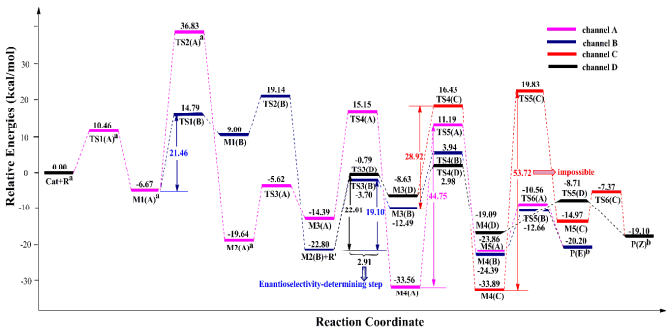

Figure 1 Energy profiles for the channels A, B, C and D (the superscripts a, b represent adding the energy of reactant R′ and catalyst Cat, respectively).

Channel A. As shown in Scheme 3, there are six tandem reaction steps in channel A.

The first step is a nucleophilic attack process. That is, the C1 atom in Cat attacks the C2 atom in the reactant R with the formation of a zwitterionic intermediate M1(A) via transition state TS1(A). The C1–C2 bond forms in intermediate M1(A) with the C1 atom approaching the C2 atom.

The analyses of NBO charges distributed on the atom (C2) and groups (Cat and R) performed at the M05-2X/6-311++G(2d,2p)//M05-2X/6-31G(d, p) level are summarized in Table 1. The negative charge distributed on the C2 atom has increased significantly from -0.30 e in R to -0.49 e in M1(A) as the nucleophilicity of the C2 atom is increased, which facilitates the following proton transfer and nucleophilic attack processes. Additionally, by comparing the charge distributed on groups (Cat and R) in the reactant (Cat+R)and in the intermediate M1(A), it is revealed that 0.81e is transferred from catalyst Cat to reactant R during the formation of M1(A), indicating that this is a nucleophilic attack process.

Table 1 NBO charges distributed on the C2 atom and some groups in Cat+R and intermediate M1(A) calculated at the M05-2X/6-311++G(2d,2p)//M05-2X/6-31G(d, p) level. (unit: e)

	C2	Cat	R
(Cat+R)	-0.30	0	0
M1(A)	-0.49	0.81	-0.81

The second step is a direct intramolecular 1,2-H shift process, through which the intermediate M1(A) is tautomerized to the intermediateM2(A) via transition state TS2(A). To be specific, with the break of C2–H4 bond and the formation of C3–H4 bond, the H4 proton transferred from the C2 atom to the C3 atom in M2(A). Notably, there is a three-membered ring configuration (C2H4C3) in TS2(A). The high strain energy contained in the three-membered ring makes the reaction hard to proceed. As shown in Figure 1, the energy barrier for this step is 43.50 kcal/mol, indicating that the direct intramolecular 1,2-H shift process is unlikely to take place under the experimental conditions.

The obtained intermediate M2(A) then reacts with another reactant MMA (R′) molecule and forms a zwitterionic intermediate M3(A) via transition state TS3(A). This is also a nucleophilic attack process. That is, with the C2 atom in M2(A) approaching the C2′ atom in R′ gradually, the C2–C2′ bond forms in M3(A). After this, a direct intramolecular 1,3-H shift process takes place, through which the intermediate M3(A) is transformed to the intermediate M4(A) via a transition state TS4(A) containing a four-membered ring. Specifically, with the breaking of the C2–H5 bond, the C3′–H5 bond forms in M4(A). Fifthly, a zwitterionicintermediate M5(A) is formed via a direct intramolecular 1,2-H shift process associated with a transition state, TS5(A), containing a three-membered ring configuration (C3H4C2). Like the second step, where there was also a transition state with a three-membered ring structure, the energy barrier of 44.75 kcal/mol in this step is also very high. In the last step, the C1-C2 bond in M5(A) is cleaved via a transition state, TS6(A), leading to the dissociation of the final product P(E) and the catalyst Cat.

Figure 1 illustrates the potential energy profile for channel A. The highest energy barrier is associated with the transition state TS5(A) (44.75 kcal/mol), which apparently is too high for the reaction to occur along channel A under the experimental conditions. The optimized structures and geometrical parameters of the reactant, transition states, intermediates and product involved in channel A are shown in Figure 2. The changes of geometrical parameters are discussed in detail in the supporting information (Part S1).

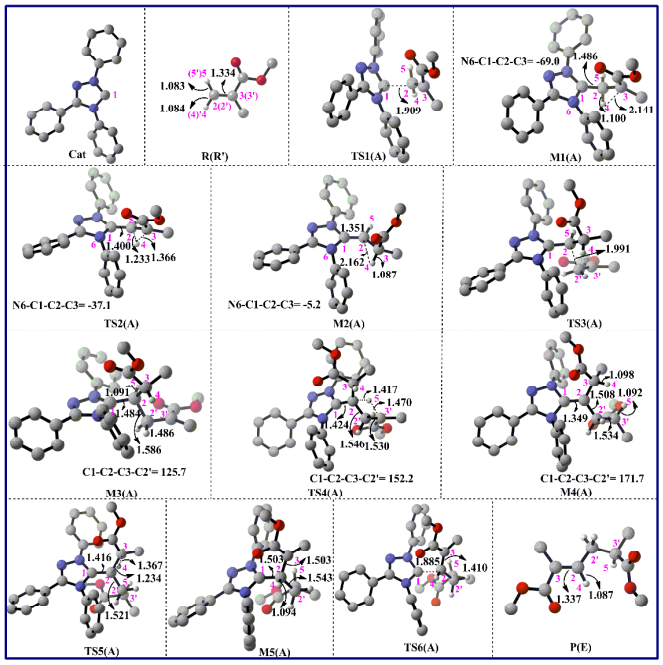

Figure 2 The optimized structures and geometrical parameters of reactant R(R′), the catalyst Cat, intermediates M1(A), M2(A), M3(A), M4(A), and M5(A), transition states TS1(A), TS2(A), TS3(A), TS4(A), TS5(A), and TS6(A), and products P(E) (hydrogen atoms not involved in reaction sites are omitted; bond lengths in angstrom; dihedral angles in degree).

Channel B. As shown in Scheme 3, there are also six reaction steps in channel B. The detailed reaction processes of channel B have been illustrated as follows:

The first step is the formation of a zwitterionic intermediate M1(A) accomplished by the nucleophilic attack of the C1 atom in Cat to the C2 atom in R via transition state TS1(A), note that this is the same as the first step in channel A. Subsequently, as M1(A) approaches another reactant R′, the intermediate M1(B) was formed via a transition state TS1(B) containing a seven-membered ring (C2C3C6O7C6′O7′H5), where the H5 proton has been transferred from the C2 atom to the O7′ atom and the C6′–O7 bond forms. In the third step, the H5 proton has been transferred from the O7′ atom to the C3 atom to form the intermediate M2(B)+R′ via the six-membered ring (C3C6O7C6′O7′H5) transition state TS2(B) as the C6′–O7 bond breaks. Noteworthy, the 1,2-H shift, that is, the H5 proton transferring from the C2 atom to the C3 atom is assisted by the reactant R′. It is worth mentioning because of the low energy of intermediate M2(B)+R, it should be able to exist for a long time and this is confirmed by the fact that it has been detected in the experiment.[13]

As shown in Figure 1, the barrier energy for the second and third steps in channel B is 21.46 kcal/mol and 10.14 kcal/mol, respectively, indicating that the reaction can proceed at the experimental temperature along this pathway. Moreover, as the energy of M2(B)+R′ is 16.13 kcal/mol lower than that of M1(A), the process of the tautomerization from M1(A) to M2(B) is exothermic. The fourth step is a nucleophilic attack process, where the C2 atom in intermediate M2(B) attacks the C2′ atom in the reactant R′ and form a zwitterionic intermediate M3(B) via transition state TS3(B).

Fifthly, a direct intramolecular 1,4-H shift occurs. To be specific, the intermediate M3(B) is tautomerized into intermediate M4(B) via the H5 proton transferring from the C3 atom to the C3′ atom associated with the five-membered ring transition state TS4(B). In the final step, the product P(E) is released from M4(B) via TS5(B) accompanied by the recovery of catalyst (Cat).

As can be seen from the potential energy profile for channel B in Figure 1, the highest energy barrier for channel B is 21.46 kcal/mol, which is associated with the transition state TS1(B), this energy barrier is much lower than that of the channel A, therefore, channel B is much more energetically favourable than channel A for the title reaction. The optimized structures and geometrical parameters of the stationary points involved in channel B are shown in Figure 3. The changes of geometrical parameters are depicted in detail in supporting information (Part S2).

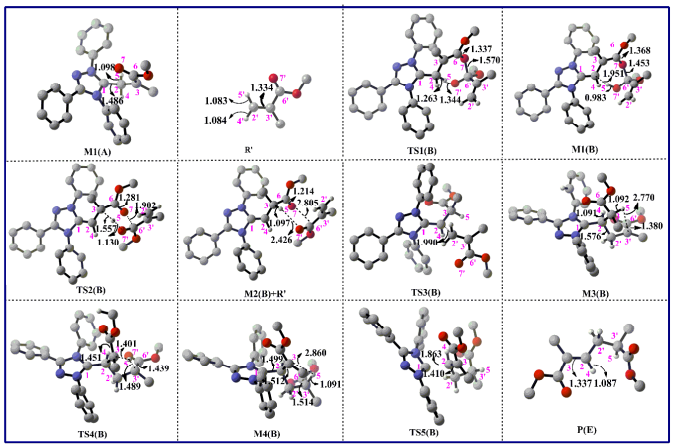

Figure 3 The optimized structures and geometrical parameters of the reactant R′, intermediates M1(A), M1(B), M2(B)+R′, M3(B), and M4(B), transition states TS1(B), TS2(B), TS3(B), TS4(B), and TS5(B), and product P(E) (hydrogen atoms not involved in reaction sites are omitted; bond lengths in angstrom; dihedral angles in degree).

Notably, the intermediate M2(B) (which is the configurational isomer of intermediate M2, depicted in Scheme 2) is involved in channel B, but the intermediate M4 (depicted in Scheme 2) detected in experiment[13] is not involved in channel B. In order to verify the appearance of intermediate M4 or its configurational isomer in the reaction and to explain the stereoselectivity of the reaction, we have suggested and studied channels C and D. Channel C and channel D are both proposed on the basis of channel B and are illustrated as follows.

Channel C. The proposed channel C is demonstrated in detail in Scheme 3. The first four steps of channel C are the same as those of channel B. In this section, we will focus on the fifth to the seventh steps of channel C:

The fifth step is a direct intramolecular 1,3-H shift process. To be specific, it is the tautomerization of the intermediate M3(B) to the intermediate M4(C) via the H4 proton transferring from the C2 atom to the C3′ atom associated with the four-membered ring transition state TS4(C). In the sixth step, a direct intramolecular 1,2-H shift process occurs. Specifically, a zwitterionic intermediate M5(C) is formed with the H5 proton transferring from the C3 atom to the C2 atom via a transition state, TS5(C), with a three-membered ring configuration. As shown in Figure 1, the energy barrier for this step is 53.72 kcal/mol, attributing to the strain of the three-membered ring in the transitional state TS5(C). In the seventh step, the final product P(Z) was obtained by the regeneration of the catalyst Cat via transition state TS6(C).

The potential energy profile for channel C (as shown in Figure 1) shows that the energy barrier associated with the transition state TS4(C) is 28.92 kcal/mol, which can be easily overcome under the experimental conditions, therefore the intermediate M4(C) (the configurational isomer of intermediate M4 depicted in Scheme 2) should be relatively easily obtained. However, the energy barrier of the rate-determining step (direct intramolecular 1,2-H shift process) for channel C is 53.72 kcal/mol, indicating that the Z-isomer product P(Z) is very difficult to be formed along channel C. The optimized structures and the geometrical parameters of intermediates M4(C) and M5(C), transition states TS4(C), TS5(C), and TS6(C), and product P(Z) are shown in Figure 4. The changes of geometrical parameters are discussed in detail in the supporting information (Part S3).

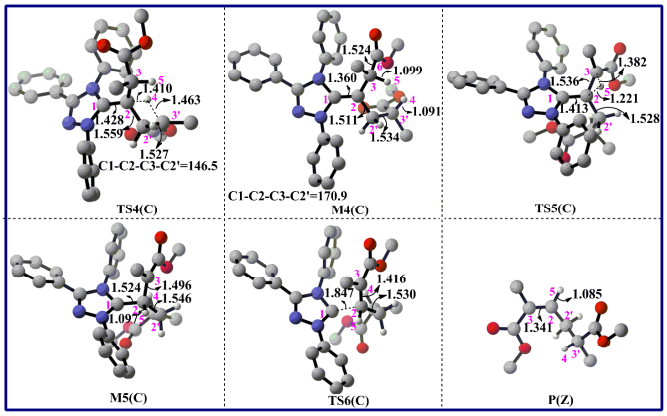

Figure 4 The optimized structures and geometrical parameters of intermediates M4(C) and M5(C), transition states TS4(C), TS5(C), and TS6(C), and product P(Z) (hydrogen atoms not involved in reaction sites are omitted; bond lengths in angstroms; dihedral angles in degree).

Channel D. There are six reaction steps in channel D, the first three are the same as those of channel B, and therefore we only discussed the last three reaction steps (the fourth step to the sixth step) in this section.

The fourth step was a nucleophilic attack of the C2 atom of the intermediate M2(B) on the C2′-C3′ double bond of reactant R′ via transition state TS3(D), leading to the formation of a zwitterionic intermediate M3(D), a configurational isomer of the intermediate M3(B) (S configuration for the C2 atom). The intermediates M3(B) and M3(D) are in fact diastereomers,, both of which contain two chiral atoms (C2 and C3) and cannot be converted into each other by the rotation of the C2–C2′ bond. The fifth step is a direct intramolecular 1,4-H shift process. The intermediate M3(D) was transformed to the intermediate M4(D) via a five-membered ring transition state TS4(D), and finally release of the product P(Z) and catalyst Cat.

As shown in the potential energy profile of channel D (Figure 1), the highest energy barrier for the entire pathway is 22.01 kcal/mol, suggesting that this pathway is energetically accessible under the experimental conditions. The optimized structures and the geometrical parameters of M2(B)+R′,

TS3(D), M3(D), TS4(D), M4(D), TS5(D) involved in channel D are shown in Figure 5. The changes of geometrical parameters are described in detail in the supporting information (Part S4).

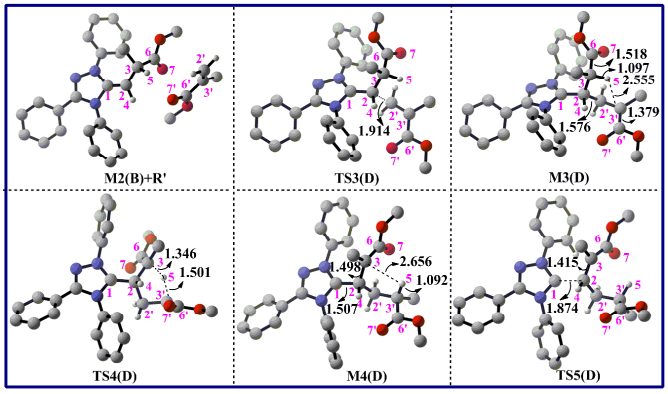

Figure 5 The optimized structures and geometrical parameters of intermediates M2(B)+R′, M3(D), M4(D), transition states TS3(D), TS4(D), and TS5(D) (hydrogen atoms not involved in reaction sites are omitted; bond lengths in angstrom; dihedral angles in degree).

Noteworthy, we have considered also the possible proton transfers assisted by zwitterionic intermediates, such as M1(A), M3(A) and M5(A). However, we have tried many times but failed to locate the proton transfer transition state assisted by them. In addition, it should be noted that the structural parameters of TS1(B) seem to be adequate and the activation barrier is reasonable. Considering that the concentration of MMA in the reaction mixture is probably significantly higher than that of intermediates, we think the intermolecular mechanism of the H-transfer proposed in our work is quite possible.

Stereoselectivity of the reaction.

As discussed above, the highest energy barriers for channels A, B, C, and D are 44.75, 21.46, 53.72, and 22.01 kcal/mol (depicted in Figure 1), respectively. Channels B and D are much more energetically favourable than the other two reaction channels (A and C). Channel B leads to the formation of the E-isomer product P(E), while channel D leads to the formation of the Z-isomer product P(Z). Obviously, the two channels (B and D) are close competitive reaction pathways in terms of energy.

How can the stereoselectivity of the reaction generate? Noteworthy, the energy favorable channels B and D share the same reaction processes associated with the transformation from reactant R and catalyst Cat to intermediate M2(B)+R′. Sequentially, M2(B)+R′ is tautomerized to E-isomer product P(E) via channel B, and is transformed into the Z-isomer product P(Z) via channel D, respectively. Comparing the optimized structures of intermediates and transition states involved in channel B and channel D (Figure 3 and Figure 5), it is easy to find that the stereoselectivity can be generated by the nucleophilic attack processes associated with the transition state TS3(B) in channel B and the transition state TS3(D) in channel D, respectively. The approaching of the reactant R′ to different faces (either Re or Si face) of the intermediate M2(B) will lead to different stereoselective configurations of the transition states including TS3(B) (S configuration for the C2 atom) and TS3(D) (R configuration for the C2 atom). To explain the issue clearly, we have illustrated the stereochemistry of the nucleophilic addition step in Figure 6.

Why the E-isomer product P(E) is the main stereoselective product detected in the experiment? Comparing the energy profiles of the favorable channels B and D, we realized that the nucleophilic attack step is the stereoselectivity-determining step of the title reaction and the population of M4(B) and M4(D) determine the E/Z value of the product. The energy barrier for the structural transformation from intermediate M2(B) to M4(B) in channel B is 19.10 kcal/mol, which is lower than that of the structural transformation from intermediate M2(B) to M4(D) in channel D (22.01 kcal/mol), indicating that M4(B) can be formed faster than M4(D) in kinetics. Moreover, the relative energy of M4(B) is 5.30 kcal/mol lower than that of M4(D), demonstrating that M4(B) is more stable than M4(D) in thermodynamics. In addition, M4(B) and M4(D) are impossible to interchange because of the different chiral carbon centers. On the basis of the above discussion, we conclude that the channel B is the most energetically favorable pathway and the product P(E) is the main product under the experimental conditions. These conclusions are in good agreement with the experimental results.[13]

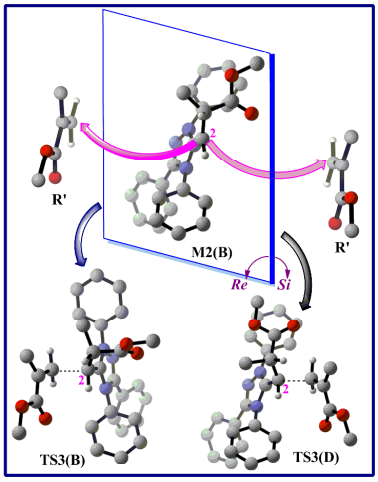

Figure 6 Illustration of the stereochemistry for channels B and D, and the optimized geometries of transition states TS3(B) and TS3(D) (hydrogen atoms not involved in reaction sites are omitted).

The role of catalyst NHC (Cat).

In order to explain the role of catalyst Cat, we have calculated and analyzed the global reactivity indices, which consist of nucleophilicity index (N) and electrophilicity index (ω). Specifically, the nucleophilicity index (N) introduced by Domingo and co-workers[22] can be used to estimate the global nucleophilicity character of a molecule, it is on the basis of the HOMO energies obtained within the Kohn-Sham scheme,[23] and defined as $N=E_{HOMO(Nu)}-E_{HOMO(TCE)}$. This nucleophilicity scale is referred to tetracyanoethylene (TCE) taken as a reference. The global electrophilicity character of a molecule is measured by the

electrophilicity index, ω,[24] following equation, $\omega = \mu^2/2\eta$, in terms of the electronic chemical potential μ and the chemical hardness η. Both quantities may be obtained in terms of the one-electron energies of the frontier molecular orbital HOMO and LUMO, ε_H and ε_L, as $\mu \approx (\varepsilon_H+\varepsilon_L)/2$ and $\eta \approx \varepsilon_L-\varepsilon_H$. Following these indices definition, the reactant R is a marginal electrophile (ω = 1.26 eV) and nucleophile (N = 1.72 eV). Our calculated results for nucleophilic index are shown in Table 2. M1(A) is an intermediate obtained from R combining with Cat (as shown in Figure 7). We can see that nucleophilicity index of M1(A) is much higher than that of R, which indicates that the catalyst Cat can catalyze the dimerization reaction by improving the nucleophilic index of reactant (R) indirectly with the formation of the intermediate M1(A).

Table 2 The nucleophilic indices of Cat, R and M1(A) calculated at M05-2X/6-311G(2d, 2p) level.

	Cat	R	M1(A)
N (eV)	3.16	1.72	5.43

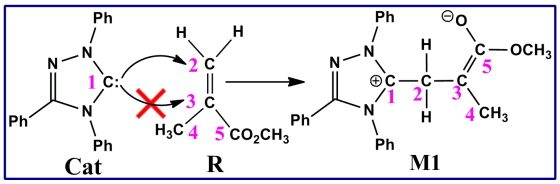

Figure 7 The catalyst Cat nucleophilic attack on the reactant R.

In order to shed light on the reaction selectivity why the C1 atom in Cat attacks on the C2 atom rather than the C3 atom in reactant R (as shown in Figure 7), we have calculated and analyzed a new local reactivity index proposed recently by Domingo et al.[25] The new local reactivity index, named Parr function P(r), is obtained from the atomic spin density (ASD) at the radical cation and at the radical anion of the corresponding reagents. The electrophilic Parr function P_k^+ and nucleophilic Parr function P_k^- for the atoms (C2, C3, C4 and C5) in reactant R were obtained through the analysis of the Mulliken ASD of the radical anion and the radical cation by single-point energy calculations at M05-2X/6-311++G(2d, 2p) level based on the optimized neutral geometries using the unrestricted formalism for radical species. The results are listed in Table 3. We find that the electrophilic Parr function and nucleophilic Parr function of C2 atom are larger than that of other atoms, which indicates that the C2 atom is more electrophilically activated than other Carbon atoms when reacting with the nucleophilic catalyst Cat.

Table 3 Electrophilic Parr function P_k^+ and nucleophilic Parr function for the atoms (C2, C3, C4 and C5) in reactant R

	C2	C3	C4	C5
P_k^+	0.56	-0.02	0.03	0.28
P_k^-	0.53	0.00	0.01	0.00

Solvation Effects

In order to confirm that the IEFPCM solvent model is suitable for this reaction system. we have compared all energetic results in channels A, B, C, D by the single-point calculations at M05-2X/6-311++G(2d, 2p) level with the solvent effect of toluene using the IEFPCM and COSMO models, which have been summarized in Table 4. The calculated results indicate that relative energies of the species obtained through different solvation models have tiny differences, therefore IEFPCM solvent model should be suitable for this reaction.

Table 4 Relative energies of the species for the dimerization at the M05-2X/6-311++G(2d,2p) level with the solvent effect of toluene using IEFPCM and COSMO models (unit: kcal/mol).

Species	IEFPCM	COSMO
TS1(A)	10.46	10.44
M1(A)	-6.67	-7.26
TS2(A)	36.83	36.47
M2(A)	-19.64	-19.00
TS3(A)	-5.62	-5.28
M3(A)	-14.39	-15.13
TS4(A)	15.15	16.11
M4(A)	-33.56	-33.12
TS5(A)	11.18	11.73
M5(A)	-23.86	-23.60
TS6(A)	-10.56	-9.72
P(E)	-20.20	-20.03
TS1(B)	14.79	15.15
M1(B)	9.00	10.27
TS2(B)	19.14	20.37
M2(B)+R´	-22.8	-22.06
TS3(B)	-3.70	-3.41
M3(B)	-12.49	-13.08
TS4(B)	3.94	3.19
M4(B)	-24.39	-24.60
TS5(B)	-12.67	-12.46

TS4(C)	16.43	17.15
M4(C)	-33.89	-33.18
TS5(C)	19.83	20.04
M5(C)	-14.97	-15.13
TS6(C)	-7.37	-6.62
P(Z)	-19.10	-18.64
TS3(D)	-0.79	-0.68
M3(D)	-8.63	-9.97
TS4(D)	2.98	2.23
M4(D)	-19.09	-20.27
TS5(D)	-8.71	-8.26
TS1(A)	10.46	10.44
M1(A)	-6.67	-7.26

Conclusions

In this work, the stereoselective reaction mechanisms (including four possible reaction channels, the E-isomer channels A and B, and the Z-isomer channels C and D) of tail-to-tail dimerization of methyl methacrylate catalyzed by N-heterocyclic carbene have been investigated theoretically using density functional theory. The E-isomer channel A followed the mechanisms proposed by Matsuoka group, which involves the direct intramolecular 1,2-H shift steps. The other E-isomer channel B, which does not involve the direct intramolecular 1,2-H shift steps, has been proposed in this work. The Z-isomer channel C, which can explain the formation of the intermediate M4 (depicted in Scheme 2) or its configurational isomer detected in the experiment, is suggested on the basis of channel B. The other Z-isomer channel D, which is the competitive reaction path with channel B, is also based on channel B. In addition, we have explained the cause of the stereoselectivity and the role of the catalyst Cat, concluding that channel B is the most energetically favorable one and the product P(E) is the stereoselective product.

The most favourable channel (channel B) contains six reaction steps as follows: The first step is the nucleophilic attack of catalyst Cat on the reactant R with formation of a zwitterionic intermediate M1(A); The second and third steps are two proton transfer processes, which make the intermediate M1(A) transform to the intermediate M2(B); Fourthly, the intermediate M2(B) nucleophilic attacks on the reactant R′ to obtain intermediate M3(B) and the stereoselectivity of the reaction occurs in this step; Fifthly, the intermediate M3(B) is tautomerized into intermediate M4(B) via the 1,4-H shift process; Finally, the product P(E) is generated with release of the catalyst Cat. Moreover, we have verified the stereoselectivity of reaction and explored the cause of the N-heterocyclic carbene catalyst Cat catalyzing the dimerization.

The obtained novel mechanistic insights should be valuable for not only understanding the reaction mechanisms of the NHC-catalyzed tail-to-tail dimerization but also the rational design of efficient and highly stereoselective NHC catalysts.

Acknowledgements

The work described in this paper was supported by the National Natural Science Foundation of China (No. 21001095).

Notes and references

[a]The College of Chemistry and Molecular Engineering, Zhengzhou University, Zhengzhou, Henan Province, 450001, PR China.
*Corresponding author. Y.Y. Zhu, E-mail address: zhuyan@zzu.edu.cn; D.H. Wei, E-mail address: donghuiwei@zzu.edu.cn.

Electronic Supplementary Information (ESI) available: List of Cartesian coordinates, E(elec), ZPVE, E(elec)+ZPVE(in Hartree, Table S1) of all stationary points involved in this work, the detailed discussion about the changes of geometrical parameters for all reaction (Parts S1-S4). See DOI: 10.1039/b000000x/

1 (a) A.J. Arduengo, R.L. Harlow and M. Kline, *J. Am. Chem. Soc.,* 1991, **113**, 361; (b)T. Zarganes-Tzitzikas, C.G. Neochoritis, J. Stephanidou-Stephanatou and C.A. Tsoleridis, *J. Org. Chem.*, 2011, **76**, 1468; (c) Y. Yamaki, A. Shigenaga, K. Tomita, T. Narumi, N. Fujii and A. Otaka, *J. Org. Chem.*, 2009, **74**, 3272; (d) O. Schuster, L. Yang, H.G. Raubenheimer and M. Albrecht, *Chem. Rev.*, 2009, **109**, 3445; (e) H. Lv, X.-Y. Chen, L.-h. Sun and S. Ye, *J. Org. Chem.*, 2010, **75**, 6973; (f) F.-G. Sun, X.-L. Huang and S. Ye, *J. Org. Chem.*, 2010, **75**, 273; (g) L. He, H. Lv, Y.-R. Zhang and S. Ye, *J. Org. Chem.*, 2008, **73**, 8101; (h) X.-L. Huang, X.-Y. Chen and S. Ye, *J. Org. Chem.*, 2009, **74**, 7585; (i) K.A. Jo, M. Maheswara, E. Yoon, Y.Y. Lee, H. Yun and E.J. Kang, *J. Org. Chem.*, 2012, **77**, 2924; (j) H. Zhou, W.-Z. Zhang, C.-H. Liu, J.-P. Qu and X.-B. Lu, *J. Org. Chem.*, 2008, **73**, 8039; (k) T.-Y. Jian, L.-H. Sun and S. Ye, *Chem. Commun.*, 2012, **48**, 10907; (l) X.-N. Wang, L.-T. Shen and S. Ye, *Chem. Commun.*, 2011, **47**, 8388; (m) L.-T. Shen, P.-L. Shao and S. Ye, *Adv. Synth. Catal.*, 2011, **353**, 1943; (n) F.-G. Sun, L.-H. Sun and S. Ye, *Adv. Synth. Catal.*, 2011, **353**, 3134; (o) C. Fischer, S.W. Smith, D.A. Powell and G.C. Fu, *J. Am. Chem. Soc.*, 2006, **128**, 1472.

2 (a) F.E. Hahn and M.C. Jahnke, *Angew. Chem. Int. Ed.*, 2008, **47**, 3122; (b) V. Nair, S. Binduand and V. Sreekumar, *Angew. Chem. Int. Ed.*, 2004, **43**, 5130; (c) S.-I. Matsuoka, *J. Syn. Org. Chem. Jpn.*, 2010, **68**, 659; (d) M. Alcarazo, T. Stork, A. Anoop, W. Thiel and A. Fürstner, *Angew. Chem. Int. Ed.*, 2010, **49**, 2542; (e) D. Enders and T. Balensiefer, *Acc. Chem. Res.*, 2004, **37**, 534; (f) W. Kirmse, *Angew. Chem. Int. Ed.*, 2010, **49**, 8798; (g) N. Marion, S. Díez-González and S.P. Nolan, *Angew. Chem. Int. Ed.*, 2007, **46**, 2988; (h) D.-C.T. Dröge and F. Glorius, *Angew. Chem. Int. Ed.*, 2010, **49**, 6940.

3 (a) X.-L. Huang, L. He, P.-L. Shao and S. Ye, *Angew. Chem. Int. Ed.*, 2009, **48**, 192; (b) L. He, T.-Y. Jian and S. Ye, *J. Org. Chem.*, 2007, **72**, 7466.
4 (a) D. Enders, O. Niemeier and A. Henseler, *Chem. Rev.*, 2007, **107**, 5606; (b) H.M. Sun, Q. Shao, D.M. Hu, W.F. Li, Q. Shen and Y. Zhang, *Organometallics*, 2005, **24**, 331.
5 W.-H. Chen, C. Wennersten, R.C.J. Moellering and S.L. Regen, *Chem. Biodivers.*, 2013, **10**, 385.
6 (a) M. Brookhart and E. Hauptman, *J. Am. Chem. Soc.*, 1992, **114**, 4437; (b) M. Brookhart and S. Sabo-Etienne, *J. Am. Chem. Soc.*, 1991, **113**, 2777; (c) K. Kashiwagi, R. Sugise, T. Shimakawa, T. Matuura, M. Shirai, F. Kakiuchi and S. Murai, *Organometallics*, 1997, **16**, 2233; (d) G.M. Direnzo, P.S. White and M. Brookhart, *J. Am. Chem. Soc.*, 1996, **118**, 6225; (e) P. Pertici, V. Ballantini and P. Salvadori, *Organometallics*, 1995, **14**, 2565; (f) T.M. Trnka and R.H. Grubbs, *Acc. Chem. Res.*, 2001, **34**, 18.
7 K. Kashiwagi, R. Sugise, T. Shimakawa, T. Matuura and M. Shirai, *J. Mol. Catal. A: Chem.*, 2007, **264**, 9-16.
8 M. Hirano, Y. Hiroi, N. Komine and S. Komiya, *Organometallics*, 2010, **29**, 3690.
9 M. Hirano, Y. Sakate, N. Komine, S. Komiya and M.A. Bennett, *Organometallics*, 2009, **28**, 4902.
10 (a) M. Doetterl and H.G. Alt, *Chemcatchem.*, 2012, **4**, 370; (b) C.-Y. Ho and L. He, *Angew. Chem. Int. Ed.*, 2010, **49**, 9182.
11 (a) A.T. Biju, M. Padmanaban, N.E. Wurz and F. Glorius, *Angew. Chem. Int. Ed.*, 2011, **50**, 8412; (b) T. Kato, S.-i. Matsuoka and M. Suzuki, *J. Org. Chem.*, 2014, **79**, 4484.
12 Y.T. Zhang, M. Schmitt, L. Falivene, L. Caporaso, L. Cavallo and E.Y.-X. Chen, *J. Am. Chem. Soc.*, 2013, **135**, 17925.
13 S.-i. Matsuoka, Y. Ota, A. Washio, A. Katada, K. Ichioka, K. Takagi and M. Suzuki, *Org. Lett.*, 2011, **13**, 3722.
14 I. Alkorta and J. Elguero, *J. Chem. Soc., Perkin Trans.*, 1998, **2**, 2497.
15 (a) D.H. Wei, M.S. Tang, J. Zhao, L. Sun, W.J. Zhang, C.F. Zhao, S.R. Zhang and H.M. Wang, *Tetrahedron: Asymmetry*, 2009, **20**, 1020; (b) K.J. Hawkes and B.F. Yates, *Eur. J. Org. Chem.,* **2008**, 5563; (c) W.J. Zhang, Y.Y. Zhu, D.H. Wei, Y.X. Li and M.S. Tang, *J. Org. Chem.*, 2012, **77**, 10729; (d) Y. Wang, X.L. Zeng and D.C. Fang, *Acta Chimica Sinica.*, 2010, **68**, 941; (e) W.J. Zhang, Y.Y. Zhu, D.H. Wei and M.S. Tang, *J. Comput. Chem.*, 2012, **33**, 715; (f) C. Zhang, Y.Y. Zhu, D.H. Wei, D.Z. Sun, W.J. Zhang and M.S. Tang, (g) *J. Phys. Chem. A*, 2010, **114**, 2913; (h) G.J. Chen, S.J. Su and R.Z. Liu, *J. Phys. Chem. B*, 2002, **106**, 1570; (i) D.H. Wei, B.L. Lei, M.S. Tang and C.G. Zhan, *J. Am. Chem. Soc.*, 2012, **134**, 10436; (j) L.R. Domingoand M. Arno, J.A. Saez, *J. Org. Chem.*, 2009, **74**, 5934; (k) D.H. Wei, W.J. Zhang, Y.Y. Zhu and M.S. Tang, *J. Mol. Catal. A: Chem.*, 2010, **326**, 41; (l) D.H. Wei, Y.Y. Zhu, C. Zhang, D.Z. Sun, W.J. Zhang and M.S. Tang, *J. Mol. Catal. A: Chem.*, 2011, **334**, 108; (m) L.R. Domingo, M.T. Picher and J.A. Saez, *J. Org. Chem.*, 2009, **74**, 2726.
16 M.J. Frisch, G.W. Trucks, H.B. Schlegel, G.E. Scuseria, M.A. Robb, J.R. Cheeseman, G. Scalmani, V. Barone, B. Mennucci, G.A. Petersson, H. Nakatsuji, M. Caricato, X. Li, H.P. Hratchian, A.F. Izmaylov, J. Bloino, G. Zheng, J.L. Sonnenberg, M. Hada, M. Ehara, K. Toyota, R. Fukuda, J. Hasegawa, M. Ishida, T. Nakajima, Y. Honda, O. Kitao, H. Nakai, T. Vreven, J.A. Montgomery, Jr, J.E. Peralta, F. Ogliaro, M. Bearpark, J.J. Heyd, E. Brothers, K.N. Kudin, V.N. Staroverov, T. Keith, R. Kobayashi, J. Normand, K. Raghavachari, A. Rendell, J.C. Burant, S.S. Iyengar, J. Tomasi, M. Cossi, N. Rega, J.M. Millam, M. Klene, J.E. Knox, J.B. Cross, V. Bakken, C. Adamo, J. Jaramillo, R. Gomperts, R.E. Stratmann, O. Yazyev, A.J. Austin, R. Cammi, C. Pomelli, J.W. Ochterski, R.L. Martin, K. Morokuma, V.G. Zakrzewski, G.A. Voth, P. Salvador, J.J. Dannenberg, S. Dapprich, A.D. Daniels, O. Farkas, J.B. Foresman, J.V. Ortiz, J. Cioslowskiand D.J. Fox, GAUSSIAN 09, Revision C.01; Gaussian, Inc.: Wallingford, CT. 2010.
17 (a) F. Huang, G. Lu, L. Zhao, H. Li and Z.-X. Wang, *J. Am. Chem. Soc.*, 2010, **132**, 12388; (b) L.L. Zhao, X.Y. Chen, S. Ye and Z.-X. Wang, *J. Org. Chem.*, 2011, **76**, 2733.
18 (a) Y. Zhao, N.E. Schultz and D.G. Truhlar, *J. Chem. Theory Comput.*, 2006, **2**, 364; (b) Y. Zhao and D.G. Truhlar, *Acc. Chem. Res.*, 2008, **41**, 157.
19 (a) K. Fukui, *Acc. Chem. Res.*,1981, **14**, 363; (b) C. Gonzalez and, H.B. Schlegel, *J. Chem. Phys.*, 1989, **90**, 2154; (c) C. Gonzalez and, H.B. Schlegel, *J. Phys. Chem.*,1990, **94**, 5523.
20 (a) B. Mennucci and J. Tomasi, J. Chem. Phys., 1997, 106, 5151; (b) B. Mennucci and J. Tomasi, J. Chem. Phys. 1997, 107, 3032.; (c) V. Barone and M. Cossi, J. Phys. Chem. A, 1998, 102, 1995.
21 (a) A.E. Reed, R.B. Weinstock and F.J Weinhold, J. Chem. Phys. 1985, **83**, 735; (b) A.E. Reed, L.A. Curtiss and F. Weinhold, *Chem. Rev.*, 1988, **88**, 899.
22 L.R. Domingo, E. Chamorro and P. Pérez, *J. Org. Chem.*, 2008, **73**, 4615.
23 W. Kohn and L. Sham, *J. Phys. Rev.*, 1965, **140**, 1133.
24 (a) R.G. Parr, L.v. Szentpály and S. Liu, *J. Am. Chem. Soc.*, 1999, **121**, 1922; (b) R.G. Parr and R.G. Pearson, *J. A m. Chem. Soc.*, 1983, **105**, 7512; (c) R.G. Parr and W. Yang, Density-Functional Theory of Atoms and Molecules; Oxford University Press: New York, 1989.
25 L.R. Domingo, P. Pérez and J.A. Sáez, *Rsc Adv.*, 2013, **3**, 1486.

